nature geoscience

ARTICLES

https://doi.org/10.1038/s41561-022-00902-9

Emergence of felsic crust and subaerial weathering recorded in Palaeoarchaean barite

Desiree L. Roerdink[1]✉, Yuval Ronen[1], Harald Strauss[2] and Paul R. D. Mason[3]

Reconstructing the emergence and weathering of continental crust in the Archaean eon is crucial for our understanding of early ocean chemistry, biosphere evolution and the onset of plate tectonics. However, considerable disagreement exists between elemental and isotopic proxies that have been used to trace crustal input into marine sediments, and data are scarce before 3 Ga. Here we show that chemical weathering modified the Sr isotopic composition of seawater as recorded in 3.52–3.20 Ga stratiform barite deposits from three different cratons. Using a combination of Sr, S and O isotope data, barite petrography and a hydrothermal mixing model, we calculate a Sr isotope evolution trend of Palaeoarchaean seawater that is much more radiogenic than the curve previously determined from carbonate rocks. Our findings suggest that evolved crust containing high Rb/Sr was subaerial and weathering into the oceans from approximately 3.7 ± 0.15 Ga onwards with impacts on ocean chemistry and the nutrient supply to the marine biosphere.

One of the most accurate and complete records for tracing the weathering of continental crust over geological time is strontium isotopes ($^{87}Sr/^{86}Sr$) in marine chemical sediments. Strontium in seawater is derived mainly from two sources with distinct radiogenic isotopic compositions: hydrothermal alteration of oceanic crust with low and mantle-like $^{87}Sr/^{86}Sr$ and subaerial weathering of continental crust with higher $^{87}Sr/^{86}Sr$[1]. Because Sr has a long residence time relative to the ocean mixing rate, $^{87}Sr/^{86}Sr$ in seawater is globally homogenized, and the balance between oceanic and continental inputs can be recorded in the Sr isotope ratios of authigenic marine minerals. Typically, the lowest (least radiogenic) carbonate $^{87}Sr/^{86}Sr$ values are taken as the best estimate of seawater at any time because post-depositional alteration is most likely to increase Sr isotope ratios[2]. Throughout the Phanerozoic eon, carbonate shells and limestones show many secular variations in seawater $^{87}Sr/^{86}Sr$ that can be linked to changes in seafloor spreading rates, as well as shifting tectonic, geographic and climatic controls on the Sr isotopic composition of riverine run-off[3]. Further back in time, the seawater Sr isotope record becomes compromised by the scarcity of unaltered sedimentary carbonate rocks. Sparse Archaean carbonates with highly unradiogenic $^{87}Sr/^{86}Sr$ have therefore been interpreted to represent seawater, suggesting a mantle-dominated ocean chemistry at this time[4,5]. This curve and the concomitant rise in seawater $^{87}Sr/^{86}Sr$ at the Archaean–Proterozoic boundary support models and proxies that argue for the late emergence of continental crust and onset of weathering around 2.5 billion years ago (Ga) (refs. [6–12]). However, recent work on two barite deposits suggested much higher seawater $^{87}Sr/^{86}Sr$ than the mantle-like value assumed from the Archaean carbonate record at 3.2 Ga (refs. [13,14]). This finding questions the assumption that the unradiogenic carbonates truly reflect seawater and challenges the validity of a mantle-like Sr isotope seawater evolution curve for the Palaeoarchaean era. The earlier onset of weathering inferred from these barite data would be consistent with Ti isotopic evidence for emerged felsic crust at 3.5 Ga (ref. [15]), weathering-induced decoupling of Hf and Nd isotope systems in 3.4 Ga chert[16] and Hf isotope ratios in black shales indicating weathering of evolved crust by 3.0 Ga (ref. [17]).

To correctly reconstruct the onset of crustal weathering and emergence of continental crust, in this article, we investigate the Sr, S and O isotopic compositions of six stratiform marine-hydrothermal barite deposits from three different cratons covering a time window of 320 Myr. Using a mixing model to assess hydrothermal influence on the barite $^{87}Sr/^{86}Sr$, we calculate a Sr isotope evolution trend for Palaeoarchaean seawater and use this result to constrain the timing at which weathering began to modify early ocean chemistry and estimate the extent of early subaerial crust.

Barite record of seawater variations

We studied field and drill-core samples from barite deposits at Londozi (3.52 Ga, Theespruit Formation), Vergelegen (3.41 Ga, Kromberg Formation), Stentor/Amo (3.26 Ga, Bien Venue Formation) and Barite Valley (3.24 Ga, Mapepe Formation) in the Kaapvaal craton, North Pole (3.49 Ga, Dresser Formation) in the Pilbara craton and Sargur (3.20 Ga, Sargur Group) in the Dharwar craton. All barite deposits occur in volcanic–sedimentary successions consistent with shallow to deep marine environments (Supplementary Table 1). Multiple sulfur isotopes provide evidence for atmospherically generated sulfate that was ultimately derived from volcanic eruptions[18–21] and probably homogenized in global seawater[19] (Supplementary Information). Measured biogenic isotope effects suggest sulfate concentrations of ~8 μM SO_4^{2-} during barite formation[22,23]. By contrast, field observations point to a hydrothermal origin for the barium[24]. In all localities, barite is strongly associated with chert[25], silica dykes feed into barite horizons at Barite Valley and North Pole[24,26], and hydrothermal alteration zones that are barium enriched relative to host rocks underlie barite at Londozi and Sargur[27,28]. However, all deposits lack polymetallic sulfide deposits, indicating that hydrothermal fluid temperatures were relatively low and probably below 150 °C (ref. [29]). Low-temperature hydrothermal activity is also consistent with the lack of an underlying magmatic system, absence of sintering and in some cases the

[1]Department of Earth Science and Centre for Deep Sea Research, University of Bergen, Bergen, Norway. [2]Institute for Geology and Paleontology, Westfälische Wilhelms-Universität Münster, Münster, Germany. [3]Department of Earth Sciences, Utrecht University, Utrecht, the Netherlands. ✉e-mail: desiree.roerdink@uib.no

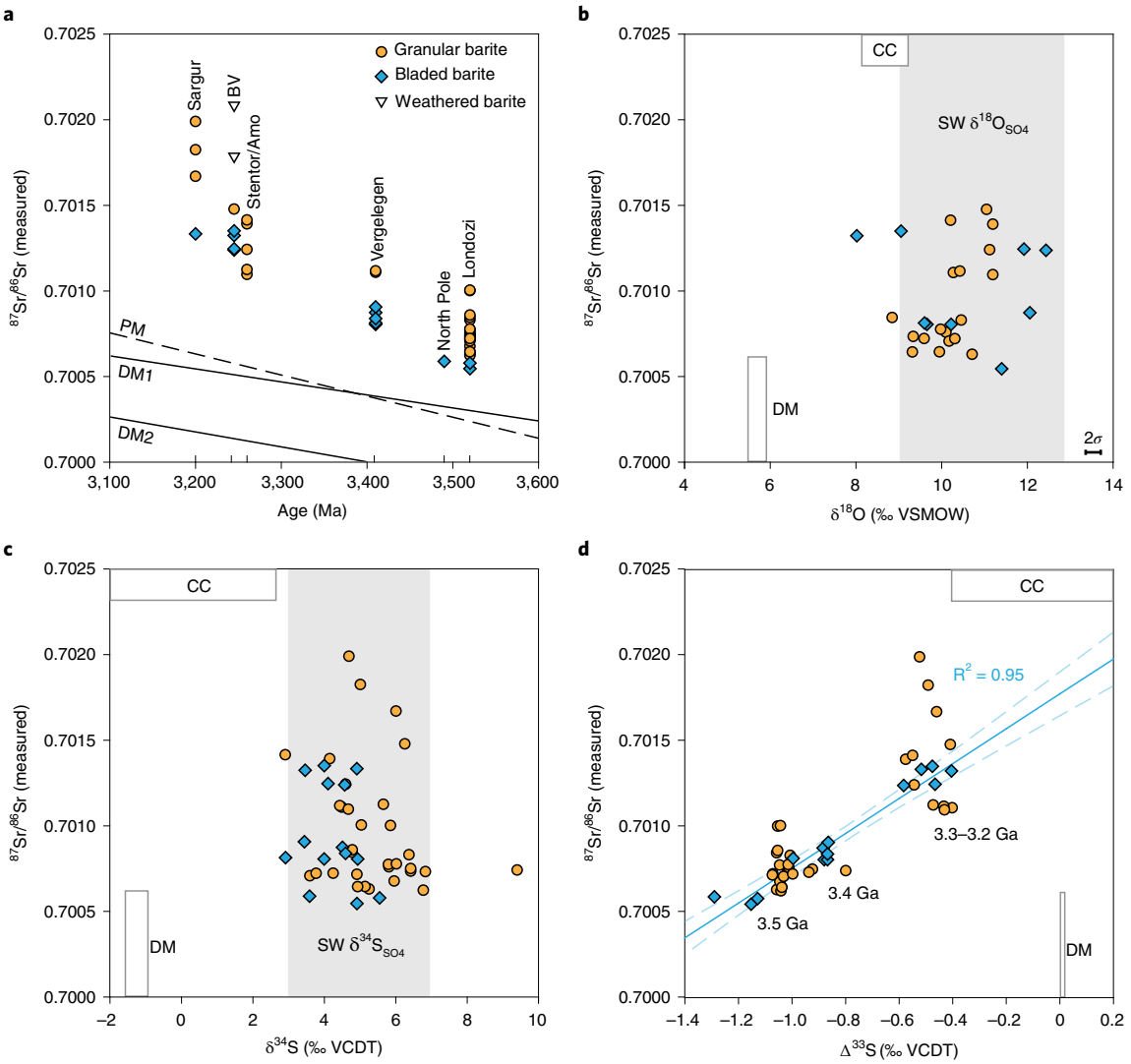

Fig. 1 | Sr, S and O isotopic compositions of Palaeoarchaean stratiform barite. a, Measured $^{87}Sr/^{86}Sr$ versus age, with depleted (DM) and primitive (PM) mantle curves. BV, Barite Valley. **b**, Measured $^{87}Sr/^{86}Sr$ versus $\delta^{18}O$ (ref. [33]), with the published range of seawater sulfate $\delta^{18}O$ indicated by the shaded region[14,18]. **c**, Measured $^{87}Sr/^{86}Sr$ versus $\delta^{34}S$ (ref. [19]), with the published range of seawater sulfate $\delta^{34}S$ indicated by the shaded region[18,34,35]. **d**, Measured $^{87}Sr/^{86}Sr$ versus $\Delta^{33}S$ (ref. [19]). Regression line (with 95% confidence intervals, dashed lines) shown for bladed barite. DM and continental crust (CC) reservoirs shown in panels **b**, **c** and **d**. Error bars are indicated when errors are larger than the symbols. References for mantle curves and reservoirs are given in Supplementary Table 11. VCDT, Vienna Cañon Diablo Troilite; VSMOW, Vienna Standard Mean Ocean Water.

small vertical extent of chert dykes[24]. Judging from mass fluxes in modern low-temperature hydrothermal systems, individual barite horizons could have formed from seawater in 10s to 100s of years (Supplementary Information).

Two types of barite are observed in the six deposits: bladed barite consisting of coarse blades up to several centimetres long and fine-grained granular barite (Supplementary Fig. 1). Crystal morphology alone does not reveal the origin of the barite. However, a combination of sedimentological evidence and morphology supports a primary origin for bladed barite at Barite Valley, except for some isolated blades cutting through barite sands that appear to have grown diagenetically[24,30]. A primary origin for bladed barite is consistent with the tabular to bladed crystal morphology that is predicted to grow in settings with low to moderate degrees of barite supersaturation[31]. By contrast, granular barite is often found in association with heavy minerals and reworked quartz, indicating a detrital origin for this morphological type[24,30]. Equigranular textures can also form by recrystallization of barite during diagenesis or metamorphism that has affected all deposits[32], from lower greenschist facies (300–400 °C) at North Pole, Barite Valley and Vergelegen to upper greenschist facies (400–500 °C) at Stentor/Amo and amphibolite facies (500–650 °C) at Londozi and Sargur (Supplementary Table 1). To determine which barite can be used to constrain Palaeoarchaean seawater $^{87}Sr/^{86}Sr$, field data and mineral morphology must be integrated with geochemical proxies.

Within individual deposits, bladed barite samples are Sr isotopically distinct from granular barite. Measured $^{87}Sr/^{86}Sr$ values are lowest in bladed barite (Fig. 1a), with weighted averages (±95% confidence intervals) ranging from 0.700562 ± 0.00015 at Londozi (n = 2), 0.700841 ± 0.00004 at Vergelegen (n = 6) and 0.701295 ± 0.00008 at Barite Valley (n = 4) to 0.701333 at Sargur (n = 1) (Supplementary Table 2). No bladed barite was found in samples from the Stentor/Amo deposit. By contrast, granular barite is characterized by higher average $^{87}Sr/^{86}Sr$ of 0.700757 ± 0.00010 at Londozi (n = 21), 0.701112 ± 0.00001 at Vergelegen (n = 2), 0.701240 ± 0.00013 at Stentor/Amo (n = 5), 0.701478 at Barite Valley

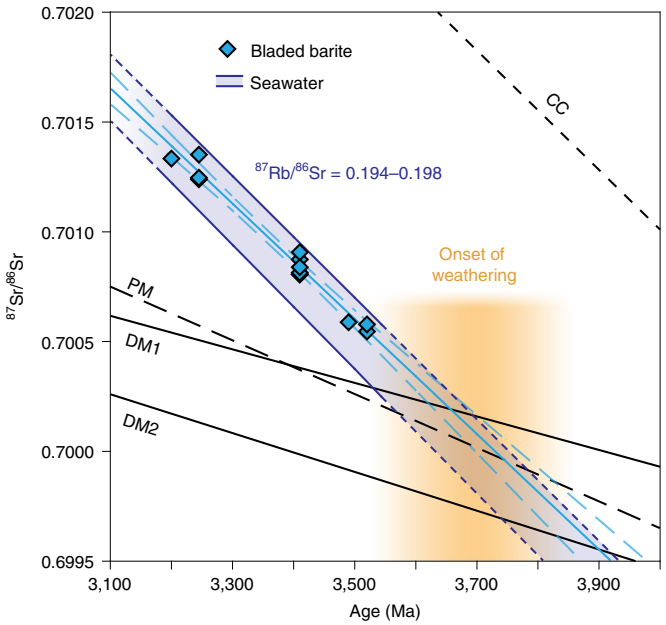

Fig. 2 | Modelled Palaeoarchaean seawater trend and the inferred onset of crustal weathering at 3.7 ± 0.15 Ga. Bladed barite $^{87}Sr/^{86}Sr$ (blue diamonds) with regression line (solid light blue curve, with dashed lines indicating 95% confidence intervals) and calculated Sr isotope evolution trend for Palaeoarchaean seawater (dark blue lines and shaded area). Dashed lines indicate extrapolation. CC, DM and PM curves are shown for reference (see text and Supplementary Information for calculation). The onset of large subaerial crustal weathering is defined from the intersection of the extrapolated seawater trend and depleted mantle curves. References for mantle and crustal curves are given in Supplementary Table 11.

($n = 1$) and 0.701814 ± 0.00033 at Sargur ($n = 3$). These higher values cannot be explained by in situ ^{87}Rb decay because measured Rb concentrations in acid-leached fractions from both types of barite are very low and would require corrections less than our analytical precision (Supplementary Table 3). In addition, we carefully selected least-weathered samples to avoid contamination with high $^{87}Sr/^{86}Sr$ phases, as exemplified by two highly weathered samples from Barite Valley (Fig. 1a).

If the Archaean oceans were homogeneous in $^{87}Sr/^{86}Sr$ due to a long Sr residence time[14], then different $^{87}Sr/^{86}Sr$ values in bladed and granular barite would not represent local isotopic variations, and only one of the two crystal morphologies may represent seawater. However, unlike the marine carbonate record, the lowest $^{87}Sr/^{86}Sr$ in bladed barite cannot be unambiguously interpreted to reflect seawater as ratios may have been lowered by hydrothermal input of unradiogenic Sr (ref. [14]). We therefore combine $^{87}Sr/^{86}Sr$ data with oxygen and sulfur isotopic compositions to select which barite is most representative of seawater (Fig. 1b–d)[19,33]. Bladed and granular barite is characterized by $\delta^{18}O$ and $\delta^{34}S$ values (see Methods for calculation, Supplementary Table 2) that fall within the range reported for Palaeoarchaean seawater from sulfate minerals and carbonate-associated sulfate (Fig. 1b,c)[14,18,34,35]. Seawater-like $\delta^{18}O$ and $\delta^{34}S$ values do not give direct evidence for seawater Sr isotope ratios in hydrothermal barite since the source of Sr is not directly coupled to that of SO_4^{2-}. However, the preceding observation is consistent with the low-temperature hydrothermal settings inferred from field data as modification of seawater-like $\delta^{18}O$ values is expected above 150 °C due to rapid oxygen isotope exchange between dissolved sulfate and water[36]. This in turn suggests that measured $^{87}Sr/^{86}Sr$ has been relatively little affected by Sr from a non-seawater source because leaching of Sr from rocks is limited at these low temperatures, and low- to intermediate-temperature hydrothermal fluids are dominated by seawater-derived Sr[37,38].

Importantly, we observe the highest $\delta^{18}O$ values for each deposit in bladed barite and in association with the most negative, and therefore most seawater-like[39], anomalous sulfur isotope signatures ($\Delta^{33}S$, see Methods for calculation, Supplementary Table 2). These samples also display a strong positive correlation ($R^2 = 0.95$) between $^{87}Sr/^{86}Sr$ and $\Delta^{33}S$ (Fig. 1d), in contrast to a weaker correlation for granular barite ($R^2 = 0.64$). Previous work has demonstrated that the magnitude of seawater sulfate $\Delta^{33}S$ decreases throughout the Palaeoarchaean, as shown in Fig. 1d[18,19]. Alternatively, these $\Delta^{33}S$ variations could reflect different photochemical reactions in volcanic plumes[21], but this does not explain the systematic correlation between $^{87}Sr/^{86}Sr$ and $\Delta^{33}S$ as atmospheric reactions do not affect Sr isotope ratios. The observed correlation between Sr and S isotopes in bladed barite is therefore best explained by co-evolution of $\Delta^{33}S$ and $^{87}Sr/^{86}Sr$ in seawater due to progressive decay of ^{87}Rb. This relationship may have been blurred in the granular barite as a result of alteration or contamination, consistent with granular textures resulting from recrystallization processes. At water/rock ratios of 1/10, metamorphic fluids with 50–1,000 ppm Sr and $^{87}Sr/^{86}Sr$ ~0.703–0.706 can shift Sr isotopic compositions from those measured in the bladed barite towards the higher values in granular barite (Supplementary Fig. 2).

On the basis of the O, S and Sr isotope systematics outlined in the preceding, we conclude that $^{87}Sr/^{86}Sr$ of the bladed barite is as close to Palaeoarchaean seawater as possible for a hydrothermal deposit. The $^{87}Sr/^{86}Sr$ values in the bladed barite define a strong regression line (Fig. 2, $R^2 = 0.98$) and are more radiogenic than two estimates for the depleted mantle based on $^{87}Sr/^{86}Sr = 0.703$ for modern mid-ocean-ridge basalt[40] and an initial value of $^{87}Sr/^{86}Sr = 0.69950$ (DM1)[8] or 0.69897 (DM2)[41] (Fig. 1a). By contrast, values are less radiogenic than the estimated Palaeoarchaean continental crust curve (Fig. 2). Our findings are consistent with previously reported Sr isotopic compositions of the Barite Valley, Sargur, Vergelegen and North Pole deposits[13,14,42]. In the following, we explore the hydrothermal influence on barite $^{87}Sr/^{86}Sr$ values to assess the Sr isotopic composition of the Palaeoarchaean oceans.

Palaeoarchaean seawater evolution trend

We use a hydrothermal mixing model (Methods) to calculate a plausible seawater Sr evolution trend from the $^{87}Sr/^{86}Sr$ values measured in bladed barite samples, based on the low-temperature hydrothermal setting inferred from field and oxygen isotope data. In our model, we calculate mixing ratios of seawater and hydrothermal fluid that lead to supersaturation with respect to barite. Our calculations for a range of Ba concentrations show that the highest degree of oversaturation occurs for a mixture consisting of 10–40% hydrothermal fluid (Supplementary Table 6). Calculated saturation indices are low (<0.2), which is consistent with our interpretation that bladed barite formed as primary crystals[31]. We use this result and a two-component mixing model to calculate $^{87}Sr/^{86}Sr$ values of seawater–hydrothermal fluid mixtures from which barite precipitated. By varying the input value for seawater $^{87}Sr/^{86}Sr$, we assess the range of seawater compositions that is feasible with the highest and lowest $^{87}Sr/^{86}Sr$ values measured in bladed barite from Londozi, Vergelegen and Barite Valley. For each deposit, we explore $^{87}Sr/^{86}Sr$ variations during hydrothermal leaching of both mafic and felsic rocks.

From our constraints on the chemical conditions required for barite precipitation and comparison of theoretical seawater–hydrothermal mixtures with those recorded in the bladed barite, we obtain a seawater Sr isotope trend with a slope corresponding to $^{87}Rb/^{86}Sr$ values of 0.194–0.198 (Fig. 2). Our empirical trend plots between modelled endmember scenarios of seawater $^{87}Sr/^{86}Sr$ for early continental growth with constant and non-constant hypsometry[12]

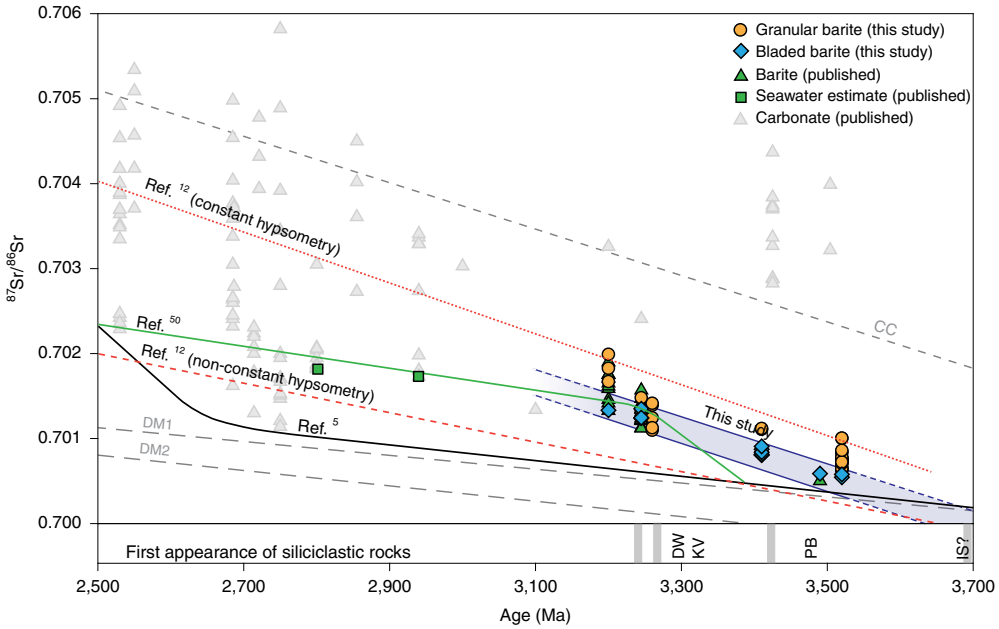

Fig. 3 | Compilation of Archaean barite and carbonate Sr isotope data and comparison with published seawater curves. Barite $^{87}Sr/^{86}Sr$ from this study (blue diamonds, yellow circles), published barite $^{87}Sr/^{86}Sr$ (green triangles)[13,14,42] and carbonate $^{87}Sr/^{86}Sr$ (grey triangles)[8,49,50] (Supplementary Table 7), and estimated seawater values (green squares)[50]. Note that the range in carbonate $^{87}Sr/^{86}Sr$ largely reflects altered samples and does not represent seawater. Our seawater Sr isotope trend (dark blue lines, shaded area) is shown in comparison with empirical (green[50] line) and modelled (black[5] line) curves[12], based on constant (red dotted line) and non-constant (red dashed line) hypsometry. DM and CC curves are shown for reference. Annotations along the lower axis indicate the first appearance of siliciclastic rocks per craton. DW, Dharwar craton; KV, Kaapvaal craton; PB, Pilbara craton; IS, Isua Greenstone Belt (Supplementary Table 8).

(Fig. 3) and Sr isotope data from North Pole, Sargur and Stentor fall well within the predicted range (Fig. 2). Calculated $^{87}Rb/^{86}Sr$ values (0.194–0.198) are substantially higher than the estimated value for the early Archaean depleted mantle (0.07 ± 0.007) (ref. [42]) and contrast strongly with the mantle-dominated curve inferred from carbonate $^{87}Sr/^{86}Sr$[4,5] (Fig. 3). This requires a supply of radiogenic Sr to Palaeoarchaean seawater from a felsic (high Rb/Sr) source[1], which is best explained by continental run-off and run-out from subaerial crust[12]. Input of Sr from submerged felsic crust was probably very limited[1] due to low seafloor weathering rates[43] and reduced further by subaqueous eruptions of flood basalts that covered continental platforms[44].

Onset of subaerial crustal weathering

The radiogenic Sr isotope values for 3.52–3.20 Ga seawater imply detectable weathering of an emerged and felsic crustal source at least 300 Myr further back in time than what has previously been reported at 3.2 Ga (ref. [14]). We further advance this by estimating the start of subaerial weathering through extrapolating our seawater evolution trend, which is notably parallel to the crustal Sr isotope curve (Fig. 2). The intersection of this trend and the depleted mantle curve at 3.7 ± 0.15 Ga represents the time at which the input of crustal Sr started to modify the $^{87}Sr/^{86}Sr$ of seawater away from mantle-dominated values and identifies the onset of notable crustal weathering. Improved constraints on the Palaeoarchaean Sr isotope mantle curve are required to further reduce the uncertainty on this estimate. However, a late Eoarchaean onset of crustal weathering is consistent with the siliciclastic rock record, which shows that physical weathering products appear for the first time in greenstone belts around 3.4 Ga and possibly as early as 3.7 Ga (Fig. 3 and Supplementary Table 8), as well as examples of exposed land surfaces by 3.5 Ga (ref. [45]) and evidence for the existence of felsic crust at this time[46].

If the extrapolation of our seawater Sr isotope trend is correct, it implies that the late Eoarchaean geodynamic regime generated granitic magmas and sufficient continental freeboard to support weathering of emerged felsic crust from 3.7 Ga. We explore this further and estimate the extent of subaerial crust for different weathering scenarios using a Sr isotope mass-balance model (Methods). Assuming a present-day area-normalized Sr weathering flux, our calculation yields an area of emerged crust of 7–12% of Earth's total surface area, comparable to the combined land areas of Europe and the Americas (Fig. 4). This scenario is consistent with limited physical erosion due to reduced topography[12] and average weathering intensities calculated for the Archaean and modern Earth[47]. However, this areal extent is substantially higher than previous estimates for the extent of emerged crust (2–5%) that were based on crustal evolution modelling[12] and oxygen isotope records[6,10] and interpreted as a Palaeoarchaean water world with little crustal weathering. Mass-balance calculations demonstrate that our revised seawater $^{87}Sr/^{86}Sr$ trend can also be explained by smaller areas of emerged crust if Sr weathering fluxes were 2–10 times higher than today (Fig. 4), which is compatible with evidence for intense chemical weathering in Archaean sedimentary rocks[48].

Our findings indicate that even for formerly considered negligible extents of emerged crust, subaerial weathering was chemically important between 3.52 and 3.20 Ga with respect to Sr and substantially modified the Sr isotope budget of seawater, in contrast to its oxygen isotope composition[10]. This in turn implies that the appearance of small areas of subaerial felsic crust may have had a more substantial impact on the composition and nutrient availability of the Palaeoarchaean oceans than previously thought.

Online content

Any methods, additional references, Nature Research reporting summaries, source data, extended data, supplementary information,

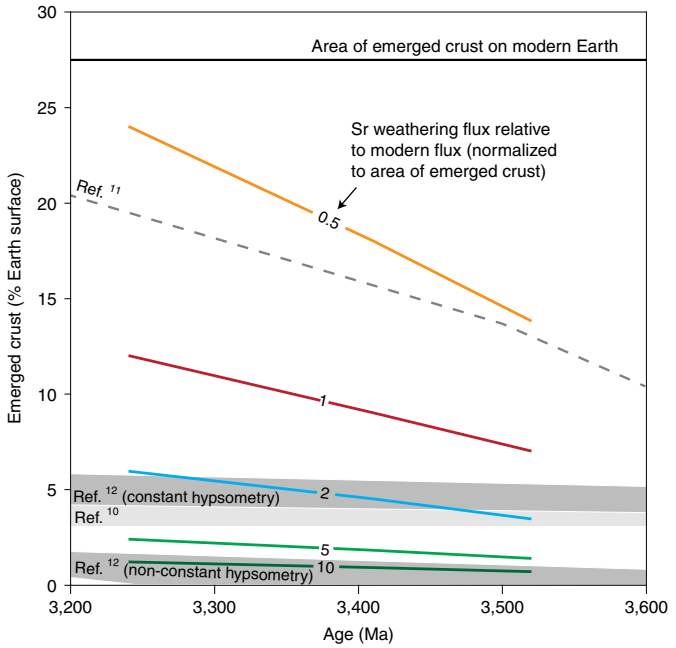

Fig. 4 | Estimated area of emerged felsic crust from 3.52 to 3.24 Ga for five weathering intensity scenarios. Area of emerged crust as percentage of the total Earth's surface area based on Sr isotope mass balance, calculated for area-normalized global Sr weathering fluxes (F_{CW}/A_{em}) of 0.5 to 10.0 times the modern flux (Methods and Supplementary Table 11). Grey dashed line and shaded areas represent previous estimates[10–12], constant hypsometry model and non-constant hypsometry model. The area of emerged crust on the modern Earth (27.5%) is shown for reference.

acknowledgements, peer review information; details of author contributions and competing interests; and statements of data and code availability are available at https://doi.org/10.1038/s41561-022-00902-9.

Received: 2 March 2020; Accepted: 14 January 2022;
Published online: 24 February 2022

References

1. Veizer, J. Strontium isotopes in seawater through time. *Annu. Rev. Earth Planet. Sci.* **17**, 141–167 (1989).
2. Veizer, J. & Compston, W. $^{87}Sr/^{86}Sr$ composition of seawater during the Phanerozoic. *Geochim. Cosmochim. Acta* **38**, 1461–1484 (1974).
3. Burke, W. et al. Variation of seawater $^{87}Sr/^{86}Sr$ throughout Phanerozoic time. *Geology* **10**, 516–519 (1982).
4. Veizer, J., Hoefs, J., Lowe, D. & Thurston, P. Geochemistry of Precambrian carbonates: II. Archean greenstone belts and Archean sea water. *Geochim. Cosmochim. Acta* **53**, 859–871 (1989).
5. Shields, G. & Veizer, J. Precambrian marine carbonate isotope database: version 1.1. *Geochem. Geophys. Geosyst.* **3**, 1–12 (2002).
6. Bindeman, I. et al. Rapid emergence of subaerial landmasses and onset of a modern hydrologic cycle 2.5 billion years ago. *Nature* **557**, 545–548 (2018).
7. Kamber, B. S. Archean mafic–ultramafic volcanic landmasses and their effect on ocean–atmosphere chemistry. *Chem. Geol.* **274**, 19–28 (2010).
8. Kamber, B. S. & Webb, G. E. The geochemistry of late Archaean microbial carbonate: implications for ocean chemistry and continental erosion history. *Geochim. Cosmochim. Acta* **65**, 2509–2525 (2001).
9. Pons, M. L. et al. A Zn isotope perspective on the rise of continents. *Geobiology* **11**, 201–214 (2013).
10. Johnson, B. W. & Wing, B. A. Limited Archaean continental emergence reflected in an early Archaean ^{18}O-enriched ocean. *Nat. Geosci.* **13**, 243–248 (2020).
11. Korenaga, J., Planavsky, N. J. & Evans, D. A. Global water cycle and the coevolution of the Earth's interior and surface environment. *Phil. Trans. R. Soc. A* **375**, 20150393 (2017).
12. Flament, N., Coltice, N. & Rey, P. F. The evolution of the $^{87}Sr/^{86}Sr$ of marine carbonates does not constrain continental growth. *Precambrian Res.* **229**, 177–188 (2013).
13. Ravindran, A. et al. Initial $^{87}Sr/^{86}Sr$ as a sensitive tracer of Archaean crust–mantle evolution: constraints from igneous and sedimentary rocks in the western Dharwar craton, India. *Precambrian Res.* **337**, 105523 (2019).
14. Satkoski, A. M., Lowe, D. R., Beard, B. L., Coleman, M. L. & Johnson, C. M. A high continental weathering flux into Paleoarchean seawater revealed by strontium isotope analysis of 3.26 Ga barite. *Earth Planet. Sci. Lett.* **454**, 28–35 (2016).
15. Greber, N. D. et al. Titanium isotopic evidence for felsic crust and plate tectonics 3.5 billion years ago. *Science* **357**, 1271–1274 (2017).
16. Garçon, M. et al. Erosion of Archean continents: the Sm–Nd and Lu–Hf isotopic record of Barberton sedimentary rocks. *Geochim. Cosmochim. Acta* **206**, 216–235 (2017).
17. Nebel-Jacobsen, Y., Nebel, O., Wille, M. & Cawood, P. A. A non-zircon Hf isotope record in Archean black shales from the Pilbara craton confirms changing crustal dynamics ca. 3 Ga ago. *Sci. Rep.* **8**, 922 (2018).
18. Bao, H., Rumble, D. & Lowe, D. R. The five stable isotope compositions of Fig Tree barites: implications on sulfur cycle in ca. 3.2 Ga oceans. *Geochim. Cosmochim. Acta* **71**, 4868–4879 (2007).
19. Roerdink, D. L., Mason, P. R. D., Farquhar, J. & Reimer, T. Multiple sulfur isotopes in Paleoarchean barites identify an important role for microbial sulfate reduction in the early marine environment. *Earth Planet. Sci. Lett.* **331-332**, 177–186 (2012).
20. Ueno, Y., Ono, S., Rumble, D. & Maruyama, S. Quadruple sulfur isotope analysis of ca. 3.5 Ga Dresser Formation: new evidence for microbial sulfate reduction in the early Archean. *Geochim. Cosmochim. Acta* **72**, 5675–5691 (2008).
21. Muller, E., Philippot, P., Rollion-Bard, C. & Cartigny, P. Multiple sulfur-isotope signatures in Archean sulfates and their implications for the chemistry and dynamics of the early atmosphere. *Proc. Natl Acad. Sci. USA* **113**, 7432–7437 (2016).
22. Crowe, S. A. et al. Sulfate was a trace constituent of Archean seawater. *Science* **346**, 735–739 (2014).
23. Havig, J. R., Hamilton, T. L., Bachan, A. & Kump, L. R. Sulfur and carbon isotopic evidence for metabolic pathway evolution and a four-stepped Earth system progression across the Archean and Paleoproterozoic. *Earth Sci. Rev.* **174**, 1–21 (2017).
24. Lowe, D. R., Drabon, N. & Byerly, G. R. Crustal fracturing, unconformities, and barite deposition, 3.26–3.23 Ga, Barberton Greenstone Belt, South Africa. *Precambrian Res.* **327**, 34–46 (2019).
25. Reimer, T. O. Archean sedimentary baryte deposits of the Swaziland Supergroup (Barberton Mountain Land, South Africa). *Precambrian Res.* **12**, 393–410 (1980).
26. Nijman, W., de Bruijne, K. H. & Valkering, M. E. Growth fault control of Early Archaean cherts, barite mounds and chert–barite veins, North Pole Dome, Eastern Pilbara, Western Australia. *Precambrian Res.* **95**, 247–274 (1999).
27. Roerdink, D. L., Mason, P. R. D., Whitehouse, M. J. & Brouwer, F. M. Reworking of atmospheric sulfur in a Paleoarchean hydrothermal system at Londozi, Barberton Greenstone Belt, Swaziland. *Precambrian Res.* **280**, 195–204 (2016).
28. Muller, É. et al. Primary sulfur isotope signatures preserved in high-grade Archean barite deposits of the Sargur Group, Dharwar Craton, India. *Precambrian Res.* **295**, 38–47 (2017).
29. Hofmann, A. & Harris, C. Silica alteration zones in the Barberton Greenstone Belt: a window into subseafloor processes 3.5-3.3 Ga ago. *Chem. Geol.* **257**, 221–239 (2008).
30. Heinrichs, T. K. & Reimer, T. A sedimentary barite deposit from the Archean Fig Tree Group of the Barberton Mountain Land (South Africa). *Econ. Geol.* **72**, 1426–1441 (1977).
31. Shikazono, N. Precipitation mechanisms of barite in sulfate–sulfide deposits in back-arc basins. *Geochim. Cosmochim. Acta* **58**, 2203–2213 (1994).
32. Hanor, J. S. in *Reviews in Mineralogy and Geochemistry: Sulfate Minerals: Crystallography, Geochemistry and Environmental Significance* (eds Alpers, C. N. et al.) 193–275 (Mineralogical Society of America, 2000).
33. Montinaro, A. et al. Paleoarchean sulfur cycling: multiple sulfur isotope constraints from the Barberton Greenstone Belt, South Africa. *Precambrian Res.* **267**, 311–322 (2015).
34. Paris, G. et al. Deposition of sulfate aerosols with positive $\Delta^{33}S$ in the Neoarchean. *Geochim. Cosmochim. Acta* **285**, 1–20 (2020).
35. Nabhan, S., Marin-Carbonne, J., Mason, P. R. D. & Heubeck, C. In situ S-isotope compositions of sulfate and sulfide from the 3.2 Ga Moodies Group, South Africa: a record of oxidative sulfur cycling. *Geobiology* **18**, 426–444 (2020).
36. Chiba, H. & Sakai, H. Oxygen isotope exchange rate between dissolved sulfate and water at hydrothermal temperatures. *Geochim. Cosmochim. Acta* **49**, 993–1000 (1985).

37. Wilckens, F. K., Reeves, E. P., Bach, W., Seewald, J. S. & Kasemann, S. A. Application of B, Mg, Li, and Sr isotopes in acid-sulfate vent fluids and volcanic rocks as tracers for fluid–rock interaction in back-arc hydrothermal systems. *Geochem. Geophys. Geosyst.* **20**, 5849–5866 (2019).
38. James, R. H., Allen, D. E. & Seyfried, W. Jr An experimental study of alteration of oceanic crust and terrigenous sediments at moderate temperatures (51 to 350 °C): insights as to chemical processes in near-shore ridge-flank hydrothermal systems. *Geochim. Cosmochim. Acta* **67**, 681–691 (2003).
39. Farquhar, J., Bao, H. & Thiemens, M. Atmospheric influence of Earth's earliest sulfur cycle. *Science* **289**, 756–758 (2000).
40. Salters, V. J. M. & Stracke, A. Composition of the depleted mantle. *Geochem. Geophys. Geosyst.* **5**, Q05B07 (2004).
41. Hans, U., Kleine, T. & Bourdon, B. Rb–Sr chronology of volatile depletion in differentiated protoplanets: BABI, ADOR and ALL revisited. *Earth Planet. Sci. Lett.* **374**, 204–214 (2013).
42. McCulloch, M. T. Primitive $^{87}Sr^{86}Sr$ from an Archean barite and conjecture on the Earth's age and origin. *Earth Planet. Sci. Lett.* **126**, 1–13 (1994).
43. Maher, K. The dependence of chemical weathering rates on fluid residence time. *Earth Planet. Sci. Lett.* **294**, 101–110 (2010).
44. Arndt, N. Why was flood volcanism on submerged continental platforms so common in the Precambrian? *Precambrian Res.* **97**, 155–164 (1999).
45. Buick, R. et al. Record of emergent continental crust ~3.5 billion years ago in the Pilbara craton of Australia. *Nature* **375**, 574–577 (1995).
46. Hoffmann, J. E., Zhang, C., Moyen, J.-F. & Nagel, T. J. in *Earth's Oldest Rocks* 2nd edn (eds Van Kranendonk, M. J. et al.) 133–168 (Elsevier, 2019).
47. Lipp, A. G. et al. The composition and weathering of the continents over geologic time. *Geochem. Perspect. Lett.* **17**, 21–26 (2021).
48. Hessler, A. M. & Lowe, D. R. Weathering and sediment generation in the Archean: an integrated study of the evolution of siliciclastic sedimentary rocks of the 3.2 Ga Moodies Group, Barberton Greenstone Belt, South Africa. *Precambrian Res.* **151**, 185–210 (2006).
49. Prokoph, A., Shields, G. A. & Veizer, J. Compilation and time-series analysis of a marine carbonate $\delta^{18}O$, $\delta^{13}C$, $^{87}Sr/^{86}Sr$ and $\delta^{34}S$ database through Earth history. *Earth Sci. Rev.* **87**, 113–133 (2008).
50. Satkoski, A. M., Fralick, P., Beard, B. L. & Johnson, C. M. Initiation of modern-style plate tectonics recorded in Mesoarchean marine chemical sediments. *Geochim. Cosmochim. Acta* **209**, 216–232 (2017).

Methods

Analytical. Barite powders were drilled from the same spots as used for previous multiple sulfur isotope[19] and oxygen isotope analyses[33] using a diamond microdrill. Circa 100 mg of pure barite was reacted with concentrated hydrofluoric acid (HF) to form insoluble SrF_2, which was centrifuged together with undissolved $BaSO_4$ to remove the supernatant. Strontium was subsequently leached from the residual solids with 2 N HNO_3 under sub-boiling conditions for 2 days. The dissolved fraction was purified on an Eichrom Sr Spec ion exchange resin and analysed for Sr isotopes using a Finnigan MAT 262 thermal ionization mass spectrometer at the University of Bergen. Values are normalized relative to $^{87}Sr/^{86}Sr = 0.710240$ for standard SRM987, with an error (2σ) of 0.000009. Aliquots of the supernatant after the HF dissolution step and the dissolved fraction after the 2 N HNO_3 dissolution step were analysed for Rb and Sr concentrations using a ThermoScientific Element XR inductively-coupled plasma mass spectrometer at the University of Bergen.

Oxygen isotopes were measured in a selection of barite powders from Londozi, Vergelegen and Stentor/Amo using a ThermoFinnigan TC/EA high-temperature pyrolysis unit coupled to a ThermoQuest Delta Plus XL mass spectrometer at the University of Münster[33]. Results are reported relative to Vienna Standard Mean Ocean Water (VSMOW) as $\delta^{18}O = [(^{18}O/^{16}O)_{sample}/(^{18}O/^{16}O)_{VSMOW} - 1] \times 1{,}000$ with an average analytical precision of 0.19‰ on $\delta^{18}O$. In addition, multiple sulfur isotopes were measured in samples from Sargur after converting barite into sulfide by boiling with a Thode reduction solution (concentrated HCl, HI and H_3PO_2). Isotope analyses were performed at the University of Maryland on a dual-inlet ThermoFinnigan MAT 253 following cryogenic and gas chromatographic purification. Results are reported relative to Vienna Cañon Diablo Troilite (VCDT) as $\delta^{34}S = [(^{34}S/^{32}S)_{sample}/(^{34}S/^{32}S)_{VCDT} - 1] \times 1{,}000$ and $\Delta^{33}S = \delta^{33}S - 1{,}000[(1+\delta^{34}S/1{,}000)^{0.515} - 1]$, with an average external precision of 0.1‰ on $\delta^{34}S$ and 0.02‰ on $\Delta^{33}S$ (ref. [19]).

Mixing model. Barite solubility products at 0.6 M NaCl (modern seawater salinity)[51] were approximated by linear extrapolation of experimental results at 0.2 M NaCl and 1 M NaCl and 25–250 °C (ref. [52]). The temperature of the hydrothermal fluid was estimated at 150 °C on the basis of element enrichment patterns and oxygen isotopes in similar silica alteration zones[29], and seawater temperature was estimated at 20 °C on the basis of isotopic evidence for modern-like temperatures[53]. Sulfate concentrations in seawater were constrained from the model of ref. [22] for sulfate-dependent microbial isotope effects and measured differences in $\delta^{34}S$ of 12–20‰ between barite and associated biogenic pyrite minerals[23]. We assume the same SO_4^{2-} concentration for the hydrothermal fluid as subseafloor anhydrite precipitation and thermochemical sulfate reduction were probably negligible at 150 °C. The saturation index SI was calculated as $\log Q/K_{sp}$ with $Q = [Ba^{2+}][SO_4^{2-}]$ and K_{sp} as the solubility product constant for different mixtures of hydrothermal fluid and seawater (T = 20–150 °C), assuming mixing temperatures without conductive cooling and Ba concentrations in the hydrothermal fluid and seawater at 75%, 90% and 99% of the solubility concentrations at 150 °C and 20 °C, respectively (Supplementary Table 5).

Based on the obtained mixing ratio of hydrothermal fluid (HF) and seawater (SW) during barite precipitation, barite (BA) Sr isotopic compositions were predicted using equation (1)[54]:

$$^{87}Sr/^{86}Sr_{BA} = \frac{^{87}Sr/^{86}Sr_{SW} - \left(^{87}Sr/^{86}Sr_{SW} \times \%HF\right) + \left(\frac{[Sr]_{HF}}{[Sr]_{SW}} \times {}^{87}Sr/^{86}Sr_{HF} \times \%HF\right)}{\left(1 + \left(\%HF \times \frac{[Sr]_{HF}}{[Sr]_{SW}}\right) - \%HF\right)} \quad (1)$$

with %HF as the fraction of hydrothermal fluid in the mixture during barite precipitation (0.1–0.4) and $[Sr]_{HF}/[Sr]_{SW}$ as the ratio of Sr concentrations in the hydrothermal fluid versus seawater. Results were calculated for $[Sr]_{HF}/[Sr]_{SW}$ ratios of 0.5, 1, 2 and 3 on the basis of enrichment factors observed in modern seafloor hydrothermal fluids[32]. To constrain the Sr isotopic composition of the hydrothermal fluids, we assume that Sr is derived predominantly from seawater (80%) with a small contribution from leached crust (20%), as observed in low-temperature (150 °C) hydrothermal experiments[38] and modern low- to intermediate-temperature hydrothermal fluids[37], and consistent with seawater-dominated REE patterns in Palaeoarchaean alteration zones[29]. Sr isotopic compositions of hydrothermal fluids were thus calculated from equation (2):

$$^{87}Sr/^{86}Sr_{HF} = 0.8 \times {}^{87}Sr/^{86}Sr_{SW} + 0.2 \times {}^{87}Sr/^{86}Sr_{L} \quad (2)$$

with $^{87}Sr/^{86}Sr_L$ as the isotopic composition of Sr leached from host rocks. For each deposit, barite Sr isotopic compositions were calculated for two endmember scenarios: (1) leaching of mafic rocks, with $^{87}Sr/^{86}Sr_L$ obtained from linearly extrapolating basaltic achondrite best initial (BABI) (0.69897) (ref. [41]) to the average modern mid-ocean-ridge basalt value of 0.703 (DM2) at the age of each deposit, and (2) leaching of felsic rocks, with $^{87}Sr/^{86}Sr_L$ constrained by linearly extrapolating BABI to the average modern crust value of 0.7119 (ref. [8]). Calculations were iterated for different input values of $^{87}Sr/^{86}Sr_{SW}$ to obtain the highest and lowest possible seawater Sr isotope composition that can explain the range in $^{87}Sr/^{86}Sr$ measured in bladed barite samples. No calculations were performed for Stentor/Amo and Sargur due to insufficient bladed barite samples.

Mass balance. To calculate global weathering fluxes and areas of subaerial land for the Palaeoarchaean, we assume Sr isotopic mass balance as in equation (3):

$$\left(^{87}Sr/^{86}Sr\right)_{SW} = \frac{F_H}{F_H + F_{CW}}\left(^{87}Sr/^{86}Sr\right)_H + \frac{F_W}{F_H + F_{CW}}\left(^{87}Sr/^{86}Sr\right)_{CW} \quad (3)$$

where $(^{87}Sr/^{86}Sr)_{SW}$, $(^{87}Sr/^{86}Sr)_H$ and $(^{87}Sr/^{86}Sr)_{CW}$ represent the Sr isotopic compositions of seawater, hydrothermal input and weathering inputs, and F_H and F_{CW} represent hydrothermal and continental weathering fluxes. Compared with the modern oceanic Sr isotope mass balance[1], we define the continental weathering flux as the combined continental run-off and run-out (groundwater discharge) flux because both have similar $^{87}Sr/^{86}Sr$ and require the presence of subaerial land. In addition, we assume that the diagenetic flux is negligible in the Archaean due to the scarcity of carbonate minerals in the rock record and assume the same $^{87}Sr/^{86}Sr$ for ocean floor weathering and high-temperature hydrothermal activity (combined as hydrothermal flux). We obtain $(^{87}Sr/^{86}Sr)_{SW}$ from our Sr isotope seawater curve and use the mentioned estimated composition of the depleted mantle and continental crust for hydrothermal and weathering inputs, respectively. On the basis of previously estimated hydrothermal fluxes[7], we calculate continental weathering fluxes from our Sr isotope data at 3.52 Ga, 3.41 Ga and 3.24 Ga (Supplementary Table 9) and use these results to evaluate required areas of emerged land in the Palaeoarchaean for different weathering scenarios using equation (4):

$$F_{CW}/A_{em} = \frac{F_{CW}}{A_{tot} \times f_{em}} \quad (4)$$

where F_{CW}/A_{em} represents the continental weathering flux normalized to the area of emerged crust, F_{CW} the continental weathering flux, A_{tot} the total surface area of Earth (5.1×10^8 km^2) and f_{em} the fraction of emerged crust. Modelled scenarios (Fig. 4 and Supplementary Table 10) range from 0.5 to 10.0 times the modern-day area-normalized continental weathering flux of 382 mol km^{-2} yr^{-1} Sr (combined run-off and run-out)[1] to reflect the uncertainty in weathering intensities for the Palaeoarchaean.

Data availability

Strontium isotope data obtained in this study are available in Supplementary Table 2 and the Pangaea data repository under https://doi.org/10.1594/PANGAEA.913541. We have used published Sr isotope data for Barite Valley, Sargur and North Pole barite samples from refs. [13,14,42], S isotope data for Londozi, North Pole, Vergelegen, Stentor/Amo and Barite Valley from ref. [19], and O isotope data for Barite Valley from ref. [33]. Ages of the barite deposits are from refs. [19,25–28,30]. The compilation of Archaean Sr isotope data shown in Fig. 3 is available in Supplementary Table 7 with references. Source data are provided with this paper.

References

51. Marty, B., Avice, G., Bekaert, D. V. & Broadley, M. W. Salinity of the Archaean oceans from analysis of fluid inclusions in quartz. *C. R. Geosci.* **350**, 154–163 (2018).
52. Blount, C. W. Barite solubilities and thermodynamic quantities up to 300 degrees C and 1400 bars. *Am. Mineral.* **62**, 942–957 (1977).
53. Blake, R. E., Chang, S. J. & Lepland, A. Phosphate oxygen isotopic evidence for a temperate and biologically active Archaean ocean. *Nature* **464**, 1029–1032 (2010).
54. Jamieson, J. W. et al. Precipitation and growth of barite within hydrothermal vent deposits from the Endeavour Segment, Juan de Fuca Ridge. *Geochim. Cosmochim. Acta* **173**, 64–85 (2016).

Acknowledgements

We thank A. Hoffman (University of Johannesburg, South Africa) for Sargur barite samples, S. H. Dundas for ICP-MS analyses, and J. Hoek and J. Farquhar (University of Maryland, United States) for multiple S isotope analyses. A. Beinlich, D. van Hinsbergen, H. Tsikos and M. van Zuilen are thanked for critically reading through an earlier version of the manuscript and providing constructive comments. This research was funded by the Research Council of Norway through the Centre for Geobiology (grant number 179560, D.L.R.), and fieldwork in South Africa was supported by the Dr Schürmann Foundation (grant number 46/2007 and 132/2018, P.R.D.M.).

Author contributions

D.L.R. conceived the study. D.L.R. and P.R.D.M. provided and prepared samples. Y.R. and H.S. measured data. D.L.R. and P.R.D.M. interpreted data and wrote the manuscript.

Competing interests

The authors declare no competing interests.

Additional information

Supplementary information The online version contains supplementary material available at https://doi.org/10.1038/s41561-022-00902-9.

Correspondence and requests for materials should be addressed to Desiree L. Roerdink.

Peer review information *Nature Geoscience* thanks Aaron Satkoski and the other, anonymous, reviewer(s) for their contribution to the peer review of this work. Primary Handling Editor: Rebecca Neely, in collaboration with the *Nature Geoscience* team.